Hindawi
Shock and Vibration
Volume 2022, Article ID 6568588, 17 pages
https://doi.org/10.1155/2022/6568588

Research Article

Mechanical Damage Test and Model Study of Layered Composite Rock Based on Acoustic Emission and DIC Characteristics

Xianyin Qi, Zhen Yang, Shengwei Wang, and Peng Fu

School of Urban Construction, Yangtze University, Jingzhou 434023, China

Correspondence should be addressed to Xianyin Qi; qixianyin001@163.com

Received 11 November 2021; Revised 1 June 2022; Accepted 11 June 2022; Published 30 June 2022

Academic Editor: Vittorio Memmolo

To study the mechanical damage characteristics of layered composite rocks, sandstones, and mudstones of deep tight reservoirs were used as the research objects, and layered composite class rocks were prepared by similar material model tests. Uniaxial compression tests were conducted and supplemented with AE (Acoustic Emission) system and DIC (Digital Image Correlation) system to obtain the physical and mechanical parameters such as strength and elastic modulus of the layered composite rocks. The corresponding law of AE ringing count and rock damage evolution was studied and the damage process of layered composite rock under uniaxial loading was divided into three stages: initial damage, stable damage development, and damage acceleration. Analysis of strain cloud diagrams of the DIC system revealed that the deformation characteristics of the layered composite rock under uniaxial were mainly tensile-shear-slip damage. Based on the internal damage evolution characteristics of AE and the surface damage evolution characteristics of DIC, a damage constitutive model of layered composite rocks based on the dual damage factor characterization was established, which reasonably revealed the damage evolution mechanism of internal structure development and external crack germination, extension and penetration of layered composite rocks under uniaxial compression.

1. Introduction

The field of oil and gas extraction is facing three major problems of "high stress, high temperature, and low permeability," among which the mechanical damage characteristics of deep composite reservoirs containing high reserves of shale gas, tight oil, and other unconventional oil and gas in a high-stress environment have an important impact on essential technical aspects of oil and gas extraction such as drilling, well wall maintenance and hydraulic fracturing. In this paper, the composite rock of a tight reservoir in Jimsar Basin is taken as the research object, and layered composite rock is prepared by a similar material model test and a uniaxial compression test is carried out, revealing that the mechanical properties and damage evolution mechanism of layered composite rock has important practical significance for oil and gas extraction and production. Extensive effort on the experimental research and theoretical analysis of composite rocks has been made. In the research of similar materials, due to the difficulty of obtaining rock samples under deep composite strata, the use of adhesives to bond different types of rocks cannot effectively simulate the colloidal bedding surface of layered composite rocks. To solve this problem, artificial rocks based on similar materials have been widely used. Shen et al. [1] conducted a test on the similar material ratio of sand-like rocks; Wen et al. [2] applied similar materials to study the mechanical properties and sensitivity of mudstone; Yin and Yang [3] conducted mechanical tests on layered composite class rocks using similar materials and classified them into three modes of failure: tensile damage, shear-slip damage, and vertical laminar surface damage.

In terms of experimental research, the application of the AE system to study the AE energy loss and signal value distribution inside the rock, and the application of DIC technology to study the displacement and strain field evolution on the rock surface have also been chosen by many researchers. For example, Zheng et al. [4] carried out uniaxial tests on sandstone with the application of the AE system, and a damage model was established to

quantitatively describe the evolution law and failure mechanism of the whole process. Zhang et al. [5] proposed a new shear model based on AE measurement to estimate the size of sandstone micro-cracks based on moment tensor analysis. The micro-cracks estimated by this model are similar to the real size of sandstone micro-cracks under the microscope and more accurate than the traditional model. Li et al. [6] used the HHT method to analyze the AE waveform characteristics under uniaxial conditions, and the research results showed that the compaction stage concentrated on the low-frequency part, the plastic deformation had obvious energy gathering characteristics, and the total energy of the waveform reached the peak at the critical failure of instability, reflecting the acoustic signal response law in the process of failure of coal rock. Zhang et al. [7] studied energy dissipation and crack characterization in the sandstone fracturing process by using AE and DIC systems. Xu et al. [8] investigated the fracture mechanism of sandstone under uniaxial load and established a mechanical damage model modified based on AE signals. Chai et al. [9] used the DIC system to study the deformation characteristics of rock-like materials and divided the rock damage evolution process into four stages according to the redefined damage variables. Xue et al. [10] conducted uniaxially and creep tests on sandstones with different dip angles of rock bridges and defects, and applied the DIC digital imaging system to study their time-dependent deformation, crack development, and failure modes. The results showed that the rock bridge dip angle and the time significantly affect the evolution of the strain field, which in turn alters the crack growth behavior and determines the ultimate strength and failure mechanism of the rock. Pan et al. [11] also applied DIC and AE systems to study the evolution of local strain field and energy dissipation characteristics of jointed rock in the axial compression process and found that the variation law was closely related to the joint angle. Munoz and Taheri [12] studied the development of progressive field strain in sandstone by using the DIC system and found that the change rate of local strain was related to the rate of strength degradation. Zhang et al. [13] studied the localization process of rock damage by using the DIC system and established the damage evolution equation based on DIC apparent strain analysis.

In terms of theoretical research, Ju et al. [14] established a damage constitutive framework for inelastic analysis of composite materials, focusing on the elastic-viscoplastic damage modeling and other issues. Abu Al-Rub and many other scholars have conducted a lot of studies on the elastic-viscoplastic model and anisotropic characteristics of composites [15–18]. Saeidi et al. [19] improved the strength failure criterion of transverse isotropic rock based on the anisotropy index. Leklinitsii. [20] calibrated the elastic theory of anisotropy and deduced the general equation of anisotropy material theory. Liu et al. [21] studied the damage evolution and strain relationship of layered composite rock, divided the damage and failure process of rock mass into three stages, and analyzed the damage law, failure characteristics, and stability of the layered rock. Jaeger and Cook [22] proposed the failure criterion of layered rock mass for the first time and the single weak plane theory. Bai et al. [23] proposed a function model for evaluating the stress-strain relationship of a discontinuous elastic medium body section. Tien et al. [24] proposed a new transverse failure criterion based on two different failure modes of transverse isotropic bodies. Zhao et al. [25] derived the anisotropic damage constitutive model of layered rock mass through the damage deterioration correction method and verified it. Li et al. [26] studied the distribution law of in-situ stress in the original rock of a deep mine, and the results showed that the magnitude of the three principal stresses on the original rock increased with the increase of depth, and the in-situ stress and stope stability were greatly affected by the geological structure and local structure.

The above-mentioned scholars have conducted a large number of in-depth studies on the mechanical properties, damage characteristics, and damage evolution laws of composite rocks. However, most of the studies focus on the description of the apparent damage characteristics and mechanism analysis of composite rocks and only consider the calculation and expression of single damage variables such as AE, DIC system, or CT scan. Fewer scholars have used a combination of multiple research tools to quantitatively analyze the internal and surface damage evolution mechanism of layered composite rocks.

Compared with previous studies, layered composite rock was prepared by similarity theory in this paper. The DIC principal strain cloud diagrams and strain information were obtained under uniaxial compression supplemented by DIC AE system monitoring in the whole process, and the distribution law of AE ringing signal with stress development was obtained. Based on the AE signal to characterize the evolution of rock internal damage and DIC to characterize the evolution of rock surface damage, a layered composite rock damage constitutive model characterized by dual damage factors under uniaxial compression was established.

Based on the internal damage status of the rock monitored by AE and the surface strain characteristics measured by DIC, the damage evolution models were established respectively, and the correlation of damage evolution characteristics of rock in the process of uniaxial compression was quantitatively analyzed by combining the complementarity of the two models at different stress stages. A segmental curve constitutive model of layered composite rock characterized by dual damage factors under uniaxial was established. The model is of great significance for characterizing the failure characteristics and damage evolution mechanism of layered composite rocks. The research results can be used in engineering links such as wellbore stability evaluation and hydraulic fracturing in deep oil and gas drilling, and provide a reference for the main mechanical data and failure modes of rocks.

2. Preparation of Rock-Like Specimens

2.1. Similar Material. In this study, due to the unloading of the deep original rock and other reasons, there is a lack of a standard sample. Then, sandstone and adjacent layer mudstone [27] in a compacted composite reservoir in Jimsar Basin were used as original rocks for the simulation test. The

cemented bedding surface of the layered composite rock was different from that of a weak horizontal interlayer and was regarded as a weak bedding surface regardless of thickness. At present, rock-like materials are usually prepared with cement and gypsum as cements, barite powder, quartz sand, silica fume, as aggregates mixed with other additives. The layered composite rock was cemented by two kinds of similar materials with different physical and mechanical properties. Considering the compactness and high strength of the composite rock, based on previous research [28, 29], white P32.5 ordinary portland cement was used as the cementing agent, and quartz sand was used as the aggregate. Because the limestone sandstone in the raw rock is denser and stronger than mudstone, silica powder and superplasticizer were added to the sandstone to enhance its strength to distinguish its physical and mechanical properties and color. For purpose of facilitating the classification and numbering in the follow-up tests, sandstone-like was called type A of rock, and the quality proportion of similar materials is that cement: quartz sand: silica fume: water: superplasticizer equal to 1: 0.8: 0.07: 0.30: 0.003; mudstone-like was called type B of rock, and the proportion of similar materials was cement: quartz sand: water equal to 1: 0.7: 0.5, and composite rocks were called type AB of rock. According to the similarity theory, the geometry, boundary and stress conditions, physical mechanics and other parameters of the prototype and the model are similar, while their physical and mechanical properties can be similar. According to the dimensional analysis method, without considering the gravity of the surrounding rock, the main similarities between the original rock and the rock-like rock are as follows:

$$\left.\begin{aligned} C\sigma &= CE = C\gamma Cl \\ C\mu &= C\varphi = 1 \\ C\gamma &= 1.2 \\ Cl &= 3.5 \end{aligned}\right\}. \tag{1}$$

Among them, C_σ, C_γ, C_l, C_μ, C_ϕ, C_E, correspond to the similarity coefficients of rock stress, bulk density, geometric size, Poisson's ratio, internal friction angle, and elastic modulus, respectively. According to the experimental plan, the bulk density similarity coefficient $C_\gamma = 1.2$, the geometric similarity coefficient $C_l = 3.5$, $C_\sigma = C_\gamma \times C_l = 1.2 \times 3.5 = 4.2$, the physical and mechanical parameters of the original rock and rock-like materials are shown in Table 1.

2.2. Preparation of Layered Composite Rock Specimens. During the test, to prepare the layered composite rock, according to the Engineering Rock Mass Test Method Standard [30], the $150 \times 150 \times 300$ mm rectangular mold, as shown in Figure 1, was adopted. The customized steel sheet was inserted in the middle of the mold to separate it for pouring. Placed it on a vibrating table and vibrate for 30 seconds, then pulled out the steel sheet, and continued vibrating for 15 seconds to make the bedding surface better bonded. It was covered with the plastic film and left for 24 hours. After the mold was removed, it was moved into a standard curing room for 28 days of curing, and a standard rock specimen was drilled by using the sampling method shown in Figure 2.

3. Test Equipment and Program

3.1. Test Equipment. The equipment used in this test is shown in Figure 3, and the loading method is shown in Figure 4. The loading system is HYAS-1000C triaxial rock test system, with a maximum axial load of 100 t and a maximum confining pressure of 30 MPa. The compression method is displacement loading, and the speed is 0.01 mm/s.

DS5 AE (acoustic emission) system including a computer control system, data collector, eight-channel sensors, and preamplifier was used in this experiment. When AE monitoring is applied separately, a total of eight AE sensors were arranged at the upper and lower ends of the rock. During the joint DIC monitoring, an AE sensor was arranged at the lower and upper ends of the remaining surface except for the speckled surface in front of the rock, with a total of six AE sensors. The main parameters are shown in Table 2. The DIC (Digital Image Correlation) system is a non-contact optical 3D measuring device for measuring and analyzing material displacement and strain. It is mainly composed of a computer control system, a support system, and a measuring system. The main parameters are shown in Table 3.

3.2. Test Program. In the process of experiment, HYAS-1000 C test system of rock triaxial compression was used to carry out the uniaxial test, and the DIC system was used to monitor the whole process of strain evolution of rock surface. Supplemented by AE system, the AE signals generated during the process of uniaxial compression of rock were collected in real time. Thus, the internal damage evolution and surface damage characteristics of the layered composite rock can be studied. The specimens are shown in Figure 5, and the specific parameters and numbers are shown in Table 4.

4. Test Results

4.1. Analysis of Mechanical Properties. The stress-strain curves obtained by uniaxial compression test of layered composite rock using a press system are shown in Figure 6(a), (b) and (c), and the average peak strength and modulus of elasticity are shown in Figure 7. The average peak strengths of type A, B, and AB rocks are 42.50 MPa, 33.69 MPa, 32.45 MPa, and the elastic modulus are 5.65 GPa, 4.32 GPa, 4.15 GPa, respectively. The strength and elastic modulus of type A of rock are higher than that type B of rocks by 21% and 24%. The strength and elastic modulus of type AB are slightly lower than that of B rocks by 3% and 4%, respectively.

This is due to the secondary failure of the layered composite rocks, which shows the stress-strain curve stress drop of AB rocks in Figure 6(c). The specimen began to fail before the lower strength or near the bedding surface and then expanded to the part of higher strength, showing sequential failure characteristics. The average strain of

Table 1: Main physical and mechanical parameters of original rock and similar rock specimens.

Rock type	Uniaxial compressive strength (MPa)	Elastic modulus (GPa)	Poisson's ratio	Density (g·cm^{-3})
Sandstone	182.22	20.18	0.27	2.59
Sandstone-like	43.37	5.46	0.26	2.14
Mudstone	152.71	15.43	0.31	2.48
Mudstone-like	34.26	4.27	0.30	2.03

Figure 1: Mold making.

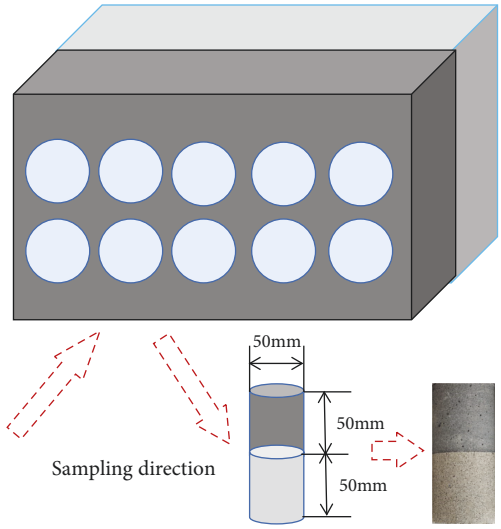

Figure 2: Sampling of layered composite rock.

compaction section of A, B, and AB rocks are 0.3%, 0.5%, and 0.6%, independently, which indicates that the type A of rocks are denser inside, the type B of rock has more micro-cracks, and the type AB of rock has slightly longer compaction section due to the existence of layered surfaces.

The failure modes of the three types of rock are shown in Figure 8, in which the transverse tensile stress of type A of rock exceeded its tensile strength due to axial compression transformation, and the cracking sound was large when the failure occurred. The shear stress of type B of rock exceeded its limit, and a small number of secondary cracks occurred at the end of the specimen. Because the bedding surface of type AB of rock produced bonding stress and constraining normal stress, part A with small deformation constrained the part B with large deformation in the composite rock. At the same time, shear stress occurred, which led to the larger deformation of part B to promote the deformation of part A. Under the coupling action of multiple factors, such as main stress, bonding normal stress at the bedding surface, shear stress, and effect of end, the rock of type AB exhibited the tension-shear slip failure along the bedding surface.

4.2. Analysis of Internal Damage Evolution of Composite Rock Based on AE. The relationship curves of AE ringing count and stress variation over time are shown in Figures 9(a)–9(c). It can be seen that AE ringing counts reflected the corresponding signal frequencies at different stress stages. After the type A of rock was compressed to the peak strength, the damage was violent and accompanied by a huge cracking sound, the strain energy was released sharply, and its AE ringing count reached 6×10^6. The AE signal inside the rock was active, which was much higher than the other two types of rock. The AE ringing count of type B rock was 1.8×10^4, which was 33.56% higher than that of type of AB rock, and the laws of AE signal in three types of rock were similar to that of strength and elastic modulus.

Based on the characteristics of AE ringing counting and stress development, such as specimen of S-6-A, the damage evolution of rock under axial compression was divided into three stages. As shown in Figure 9(a), in stage I of initial damage, the primary micro-cracks, and bedding of the rock were mainly compacted and closed, and the AE ringing signal was weak at 0–25 s, and the stress curve was concave upward. In the stage II of stable damage development, at 25~67 s, the stress curve in this stage was approximately straight, the rock was elastically deformed, and a small number of new fractures sprouted inside and developed slowly. The AE signal was more active than the compaction stage but was still not severe.

In stage III of damage acceleration, within 67~140 s, the new fractures inside the rock expanded rapidly and intersected and penetrated. The AE signal value grew rapidly, the internal damage developed continuously and produced a macroscopic crack surface outside, and the rock presented plastic failure as a whole. After reaching the peak intensity at 84 s, the AE signal reached the maximum value correspondingly. After the damage of the internal structure, the stress fell rapidly, and the AE ringing signal value decreased correspondingly. Meanwhile, the stress curves in Figure 9(c) show that the type AB of rock produced stress drop with axial pressure loading at 38 s and was accompanied by abrupt changes in AE ringing counts. The existence of secondary damage indicated that the micro-fissure on the internal bedding surface of type AB of rock started to develop, expanded, and tended to fail at this time. This is a typical damage characteristic of AE of layered composite rock, which can also be verified in Figure 8 of the failure pattern of rock specimens.

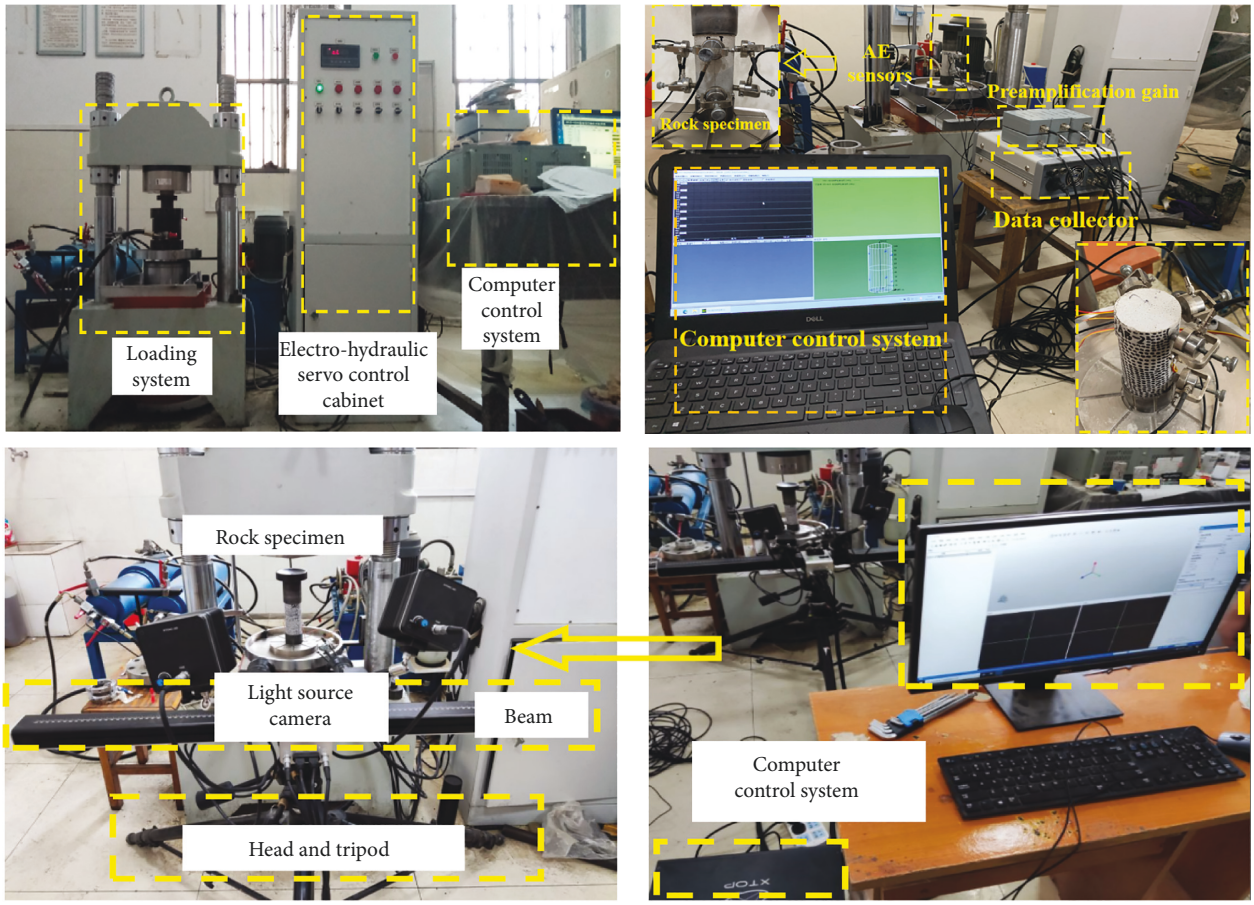

Figure 3: Test equipment.

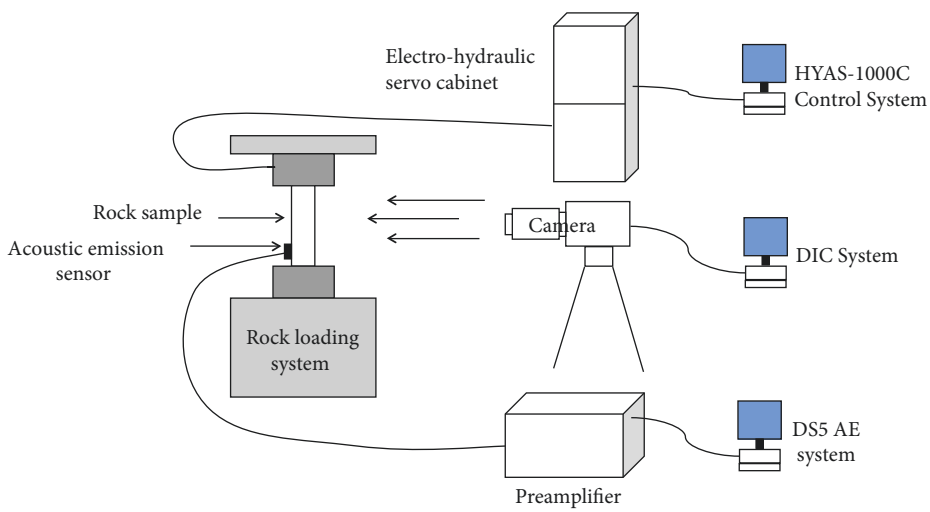

Figure 4: Loading method.

In the process of the uniaxial test, although there was occasional hysteresis in the AE ringing signal due to the AE sensor falling off with the rock debris during the damage accelerated stage, the overall evolution characteristics of the initial damage and the stable development stage of the damage inside the rock can be well described.

4.3. Surface Damage Evolution Characteristics of Composite Rock Based on DIC

4.3.1. Analysis of DIC Surface Strain Cloud Diagram. In combination with the DIC system, the surface deformation of type A, B, and AB of rock under the uniaxial test was

Table 2: Main parameters of DS5 Acoustic Emission System.

Content	Number of channels/#	Threshold (dB)	Preamplifier (dB)	Sampling frequency (kHZ)	Interface form
Parameter	8	40	40	30	USB3.0

Table 3: Main parameters of DIC system.

Content	Camera resolution (PX)	Pixel size (μm)	Frame rate (fps)	Lens focal length (mm)	Focal length of light source (mm)
Parameter	4096×3000	3.45	30	12	10

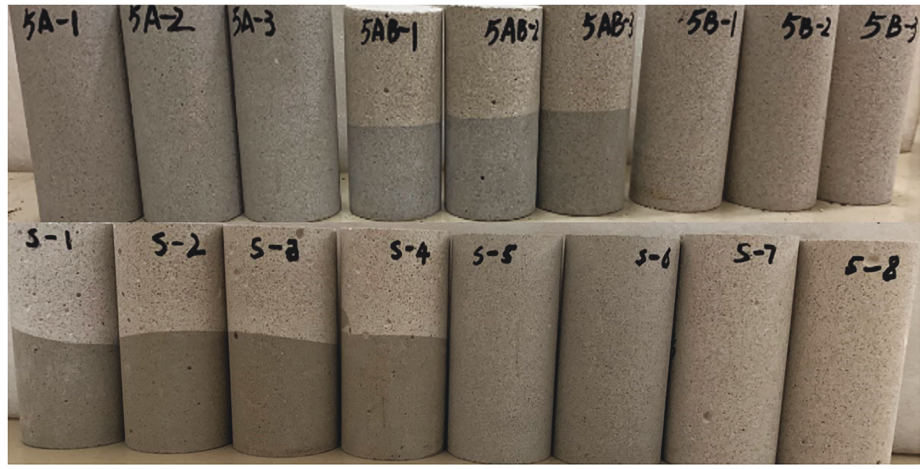

Figure 5: Layered composite rock sample.

Table 4: Parameters and numbers of specimens.

Specimens	Length (mm)	Radius (mm)	Quality (g)	Density ($g \cdot cm^{-3}$)	Test type
S-1-AB	99.82	49.15	393.38	2.08	Applied acoustic emission system monitoring
S-2-AB	99.15	49.26	391.45	2.07	
S-3-AB	99.20	49.31	392.84	2.07	
S-4-AB	98.54	49.58	393.12	2.07	
S-5-A	99.21	49.16	402.16	2.14	
S-6-A	100.12	49.25	410.72	2.15	
S-7-B	101.06	49.17	390.38	2.04	
S-8-B	101.14	49.15	390.16	2.03	
5A-1	99.15	49.12	402.54	2.14	
5A-2	101.11	49.15	413.37	2.16	
5A-3	100.56	49.16	412.02	2.15	
5AB-1	99.28	49.22	391.66	2.07	Application of DIC system monitoring, including composite rock combined with acoustic emission monitoring
5AB-2	99.15	49.13	389.72	2.07	
5AB-3	99.24	49.11	390.47	2.08	
5B-1	98.45	49.12	378.63	2.03	
5B-2	99.98	48.96	379.72	2.02	
5B-3	99.65	49.24	387.56	2.04	

monitored in real time, and the surface principal strain cloud diagram of the specimens was obtained. Due to the limitation of space, only the principal strain cloud diagrams of the primary failure modes of the three types of rock are listed, as shown in Figures 10(a)–10(c), which are the principal strain cloud diagrams and failure modes of specimens 5A-2, 5AB-2 and 5B-3, corresponding to peak strengths of 0%, 50%, 75%, and 100%, respectively.

tAs shown in Figure 10(a), when the axial stress was loaded to 50% of the peak strength, the surface of the specimen was uniformly deformed without obvious local strain. At 135 s corresponding to 75% of the peak strength, a tension crack sprouted on the right side of the middle of the specimen surface, and the strain at the crack rapidly increased to 6.762%, and a strain localization zone was generated along the axial direction, entering the plastic deformation stage. After reaching the peak strength at 179 s, the crack expanded into a tension crack with a wider middle and finer end, and the maximum strain was 7.202%, and the strain localization zone was transported to the

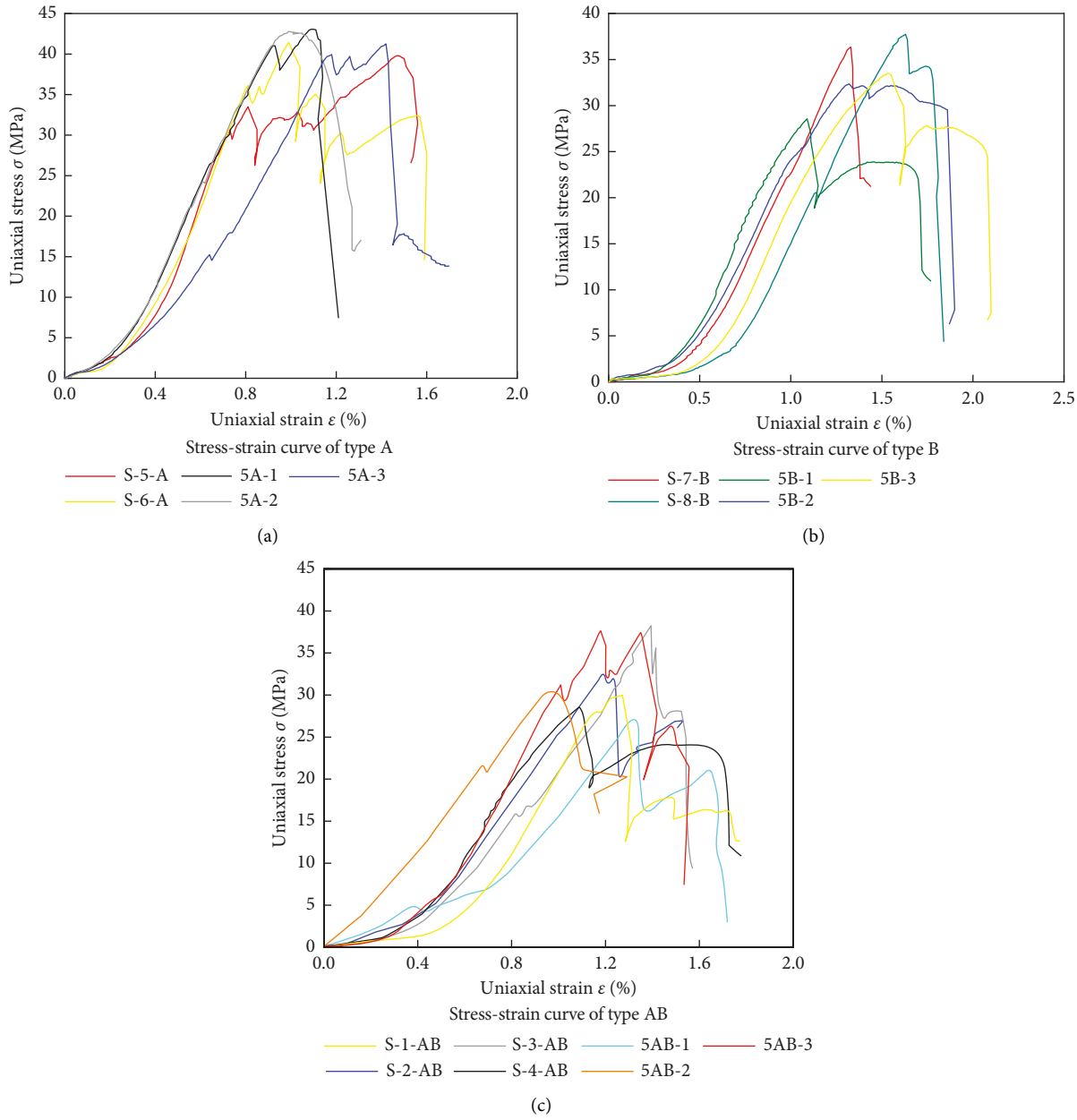

Figure 6: Stress-strain curve of rock. (a) Stress-strain curve of type A. (b) Stress-strain curve of type B. (c) Stress-strain curve of type AB.

lower right end of the specimen and the scattered spots fell off.

As shown in Figure 10(b), at 52 s corresponding to the compacting stage of rock, its principal strain increased slowly, and no cracks were generated in the observation area, and the average strain was 0.157%. With the growth of axial pressure, when the peak strength of 75% was reached at 116 s, the specimen generated non-integral shear-slip cracks along the bedding surface due to the coupling of the bonded positive stress with the main stress and end effect of the composite rock bedding surface, and the principal strain cloud diagram showed two horizontal plane with large local deformations and strain growth up to 1.120%.

At 176s, the post-peak stage was entered, and the final tension crack with strain localization zone was formed in the left part of the specimen due to factors such as rock composition, internal structure, and inhomogeneity, and the composite rock as a whole showed tension-shear slip failure.

As shown in Figure 10(c), at 82 s corresponding to 50% of the peak strength, due to the end effect, the larger deformation gathered at the bottom of the specimen, the strain reached 1.878%, which was larger than the upper strain, and the whole presented layered homogeneous deformation. At 118 s the rock entered the plastic stage, due to its internal pores, inhomogeneity and other factors, the internal stress of the rock was redistributed, and the strain gradually evolved into an inclined shear zone. At 168 s, the specimen entered the post failure stage, and the shear penetration zone along the oblique section was obvious, with a strain of 1.013%. The strain in the area not penetrated was uniform and small, and the overall

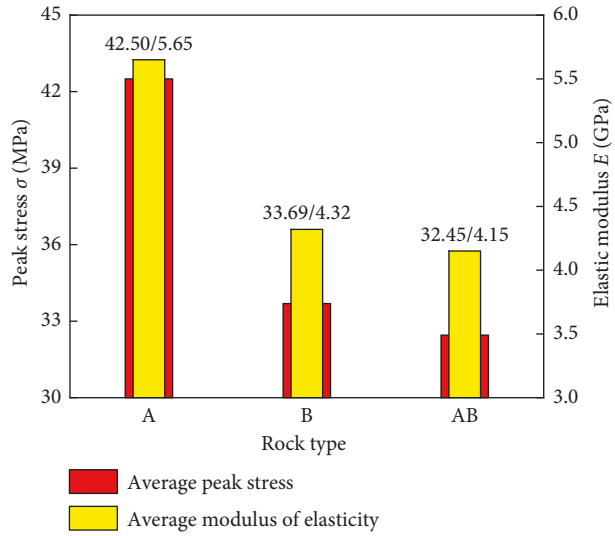

Figure 7: Average peak strength and elastic modulus of rock.

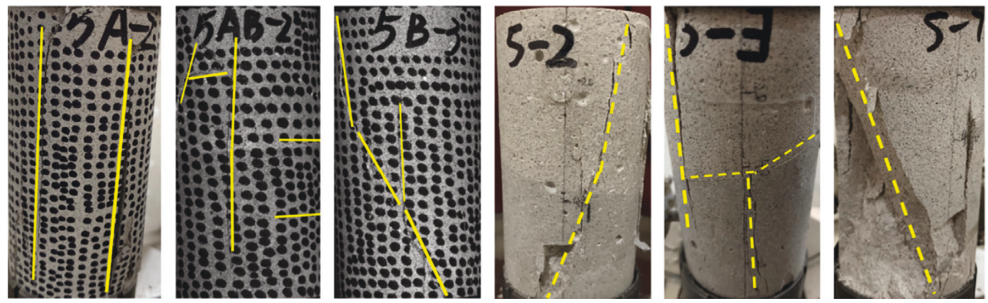

Figure 8: Deformation and failure modes of rock samples.

strain of the specimen was laminarly distributed up and down after compression and then penetrates an oblique shear zone from the left to the right bottom, which also reflected the evolutionary characteristics of shear damage.

4.3.2. Evolution Characteristics of DIC Surface Strain Points. The strain-time evolution information gathered from strain gauges and DIC of specimens 5A-2, 5AB-2, and 5B-3 are shown in Figures 11–13, respectively. The strain information of points and full on the specimen surface can be collected completely by modeling the points taken on the specimen surface within the DIC system, with each specimen in a rectangular shape and taking a total of 6 points from 0 to 5. Since the strain gauges were easily damaged when attached to the specimen surface, it was difficult to obtain the strain information of the whole process, while the strain information of the whole process can be obtained by DIC system except for the direct falling off or warping of the rock surface. Figure 11 shows that the trend of sudden variation in axial strain measured by DIC and strain gauges at 90 s and 135 s corresponding to 75% of the peak intensity was the same.

Meanwhile, Figures 12(a) and 13(a) show that the strains measured by DIC and strain gauges do not exactly match, but the overall trend is similar. This is because the DIC system reflects the dynamic evolution of local strains, while the strain gauge collects strain information within a fixed measurement area.

Figure 11(b) shows that specimen 5A-2 produced obvious localized deformation at 87s corresponding to 50% of the peak strength, while Figure 10(a) shows that points 0, 2, and 4 on the left side of the specimen were at the tension crack, resulting in approximately linear growth of its strain, and at 135s corresponding to 75% of the peak strength, the strain increased rapidly after the stress redistribution of the specimen, at which strain points 3 and 5 were on the through tension crack and had the strain information could not be collected further, and the specimen then lost its bearing capacity after brittle failure, while the strain points not in the strain localization zone continued to grow. Figure 12 shows that the strain at point 3 increased with time, but its growth rate was significantly smaller than the peak phase, which could also verify the phenomenon of shear-slip cracking on the right side of the bedding surface in the middle of the composite rock in Figure 10(b). Figure 13 shows that the strain values in different areas on the surface of specimen 5B-3 produced significant differences, and it could be seen from Figure 10(c) that with the shear zone penetration and friction on the macroscopic cracking surface, the strain at point 2 suddenly increased, and the strain growth of measurement points 0 and 1 in the upper undamaged area of the specimen was smaller, and

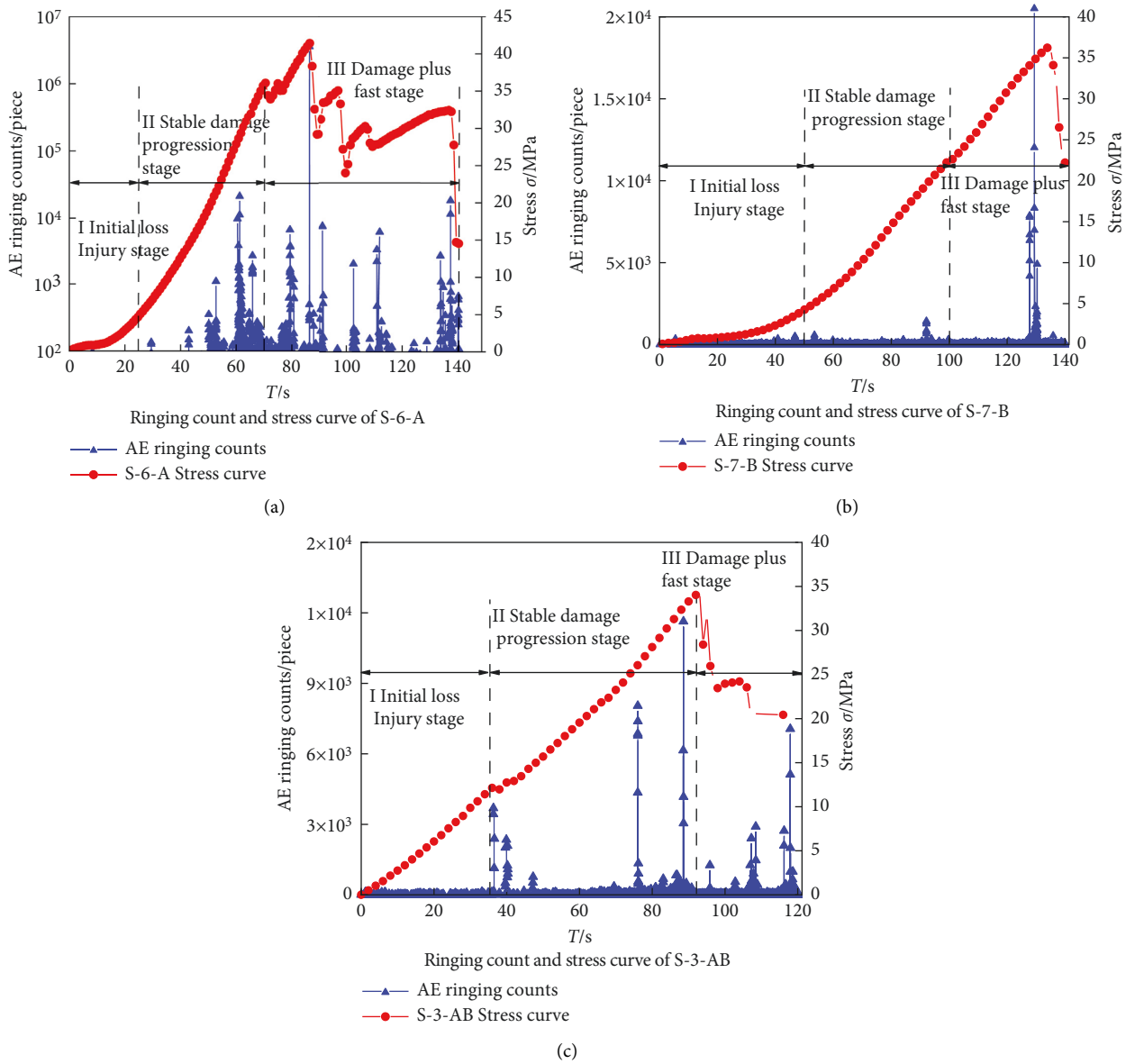

Figure 9: Curve of AE ringing count and stress-time. (a) Ringing count and stress curve of S-6-A. (b) Ringing count and stress curve of S-7-B. (c) Ringing count and stress curve of S-3-AB.

the strain values of points 4 and 5 in the lower part became larger due to the end effect.

In summary, the damage evolution of surface crack sprout, extension, and penetration in layered composite rocks can be reasonably characterized by the surface strain of rock measured by DIC.

5. Damage Constitutive Model of Layered Composite Rock Based on Dual Damage Factors' Characterization of AE and DIC Characteristics

5.1. Damage Constitutive Model Based on Characteristics of AE Ringing Count. Damage refers to the existence and development of defects, micro-cracks, pores, and beddings in rocks. With the change of external conditions, the strain energy is released and the pulse signal in the form of an elastic wave is produced. Therefore, the damage evolution process of rock can be directly characterized by quantitative calculation of AE signal in the test. The studies show that the AE ringing count is proportional to the dislocation motion and the strain energy released by the crack development of the material, and is one of the characteristic parameters in AE signals [31]. Based on Section 4.2, in this paper, AE ringing count was used as a parameter to describe the evolution characteristics of the initial damage and the stable development stage of the rock internally in a relatively reasonable manner. Kachanov. [32] defined the damage variable as the ratio of the sectional area occupied by the micro-defect to the total area of the section:

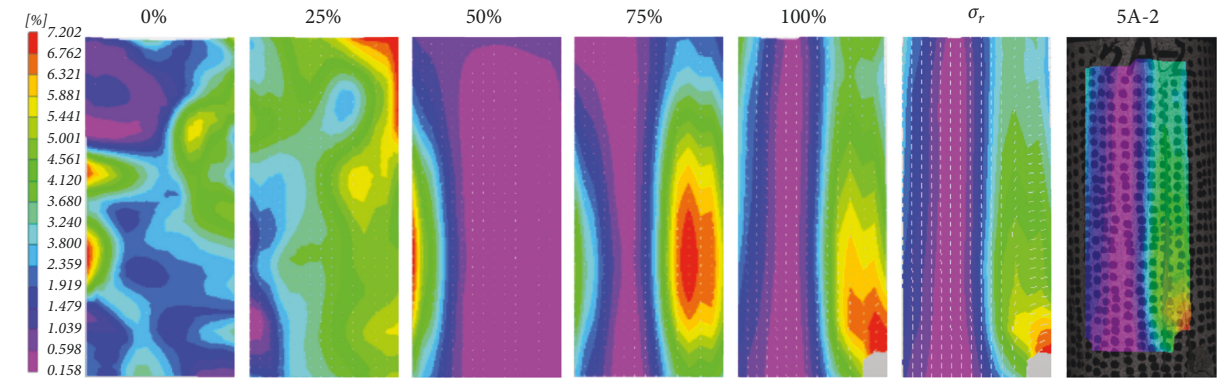

Major strain cloud diagrams of 5A-2

(a)

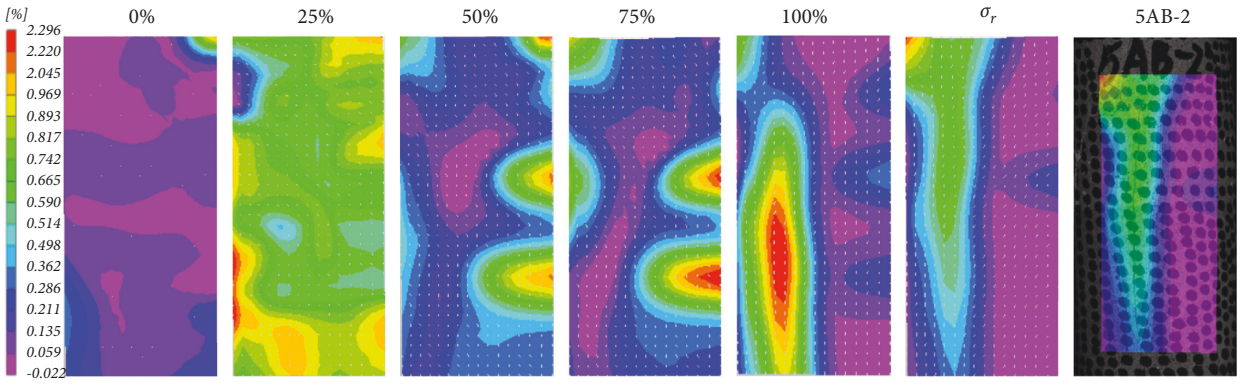

Major strain cloud diagrams of 5AB-2

(b)

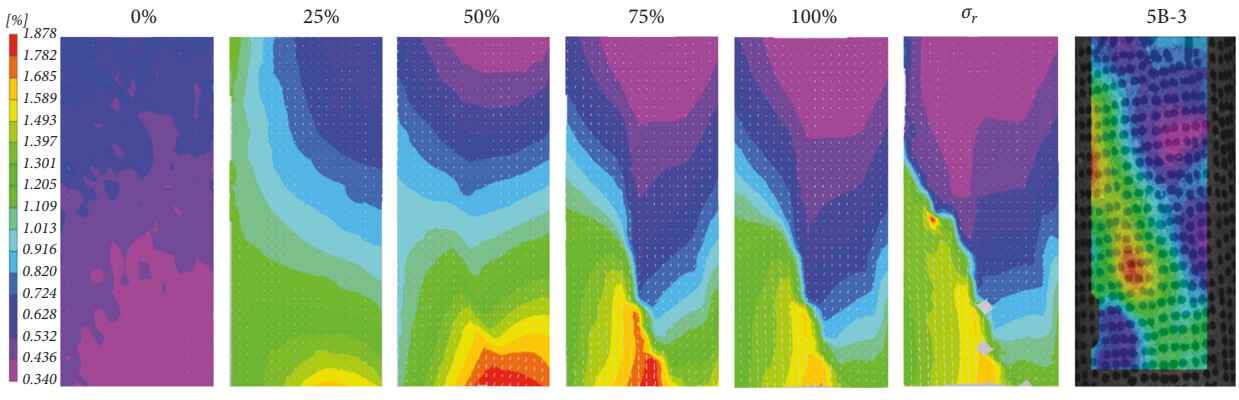

Major strain cloud diagrams of 5B-3

(c)

FIGURE 10: Major strain cloud diagrams of rock specimen. (a) Major strain cloud diagrams of 5A-2. (b) Major strain cloud diagrams of 5AB-2. (c) Major strain cloud diagrams of 5B-3.

$$D = \frac{A_d}{A}. \tag{2}$$

Among them, A_d is the area of the defect element on the bearing area of rock, and A is the initial bearing section of the rock. If the cumulative number of AE ringing is N when the initial section A is completely damaged, and the cumulative number of AE ringing is N_d when the area of the defective micro-element reaches A_d, the damage factor D_{AE} of cumulative ringing is defined as:

$$D_{AE} = \frac{N_d}{N}. \tag{3}$$

The correlated function [33] between AE cumulative ringing count and strain evolution is introduced and improved, such as:

$$N_d = k_1 \varepsilon \exp(k_2 \varepsilon). \tag{4}$$

In the Equation, k_1, k_2 are the damage index coefficient, and ε is strain. Substituting Equation (4) into Equation (3),

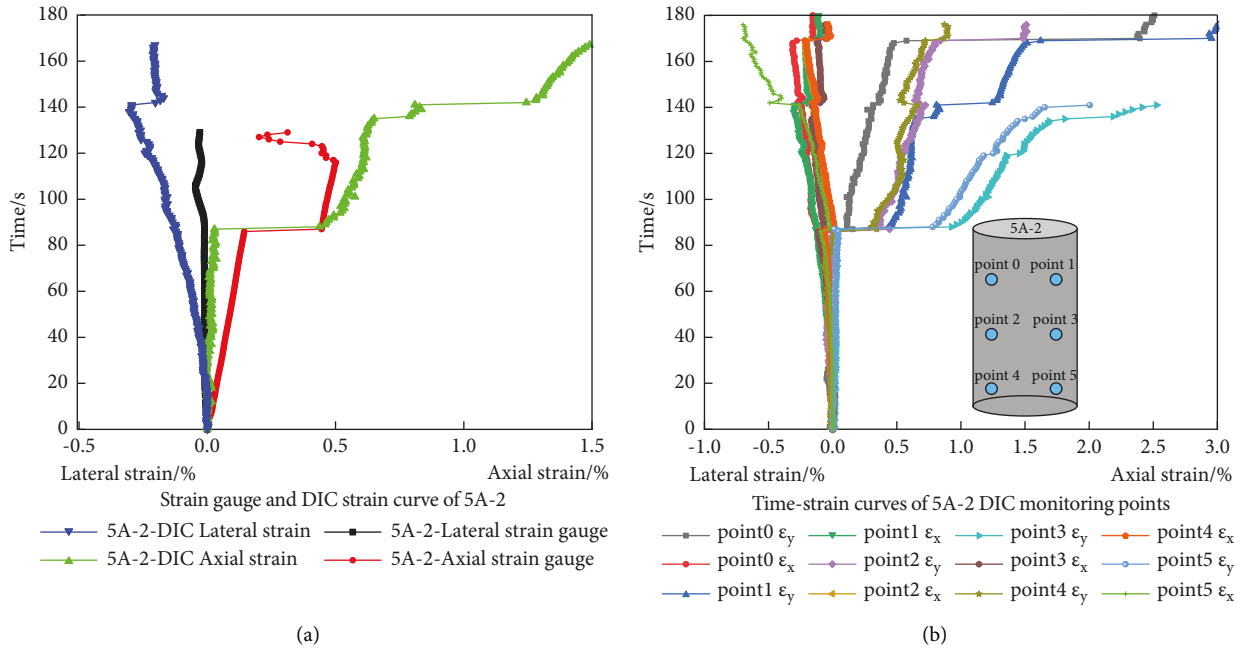

(a) (b)

FIGURE 11: Time-strain curve of 5A-2. (a) Strain gauge and DIC strain curve of 5A-2. (b) Time-strain curves of 5A-2 DIC monitoring points.

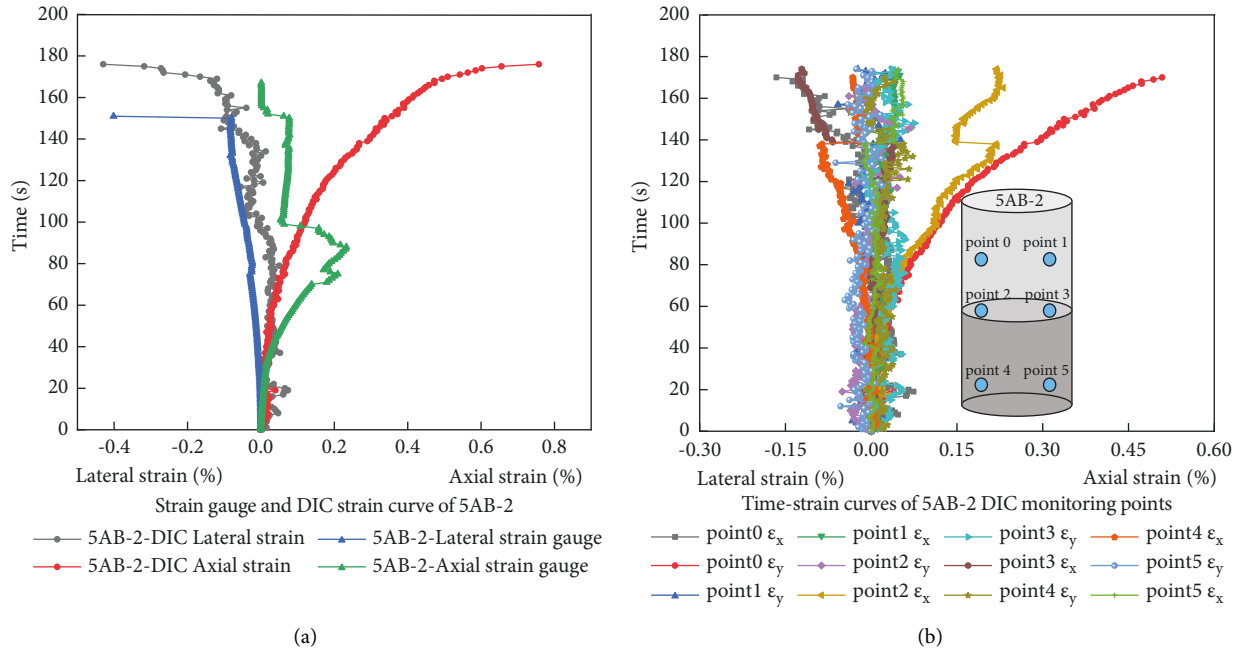

(a) (b)

FIGURE 12: Time-strain curve of 5AB-2. (a) Strain gauge and DIC strain curve of 5AB-2. (b) Time-strain curves of 5AB-2 DIC monitoring points.

the relationship between damage factor of AE cumulative ringing and strain function can be obtained as follows:

$$D_{AE} = \frac{k_1 \varepsilon \exp(k_2 \varepsilon)}{N}. \quad (5)$$

Fitting the data of specimen S-3-AB in Equation (5) shows that $k_1 = 41.129$, $k_2 = 492.741$, the damage evolution equation of damage factor D_{AE} and strain ε of layered composite rocks can be obtained (6):

$$D_{AE} = 0.031\varepsilon \exp(492.741\varepsilon). \quad (6)$$

The damage evolution curve of damage factor D_{AE} and strain ε is shown in Figure 14. Before the strain reached 0.0045, the AE signal was not active, and the D_{AE} value was small at the initial damage stage. When the strain was between 0.005 and 0.01, the damage developed steadily. New cracks were sprouted in the rock, and the strain reached 0.010, and the damage increased rapidly to 1.

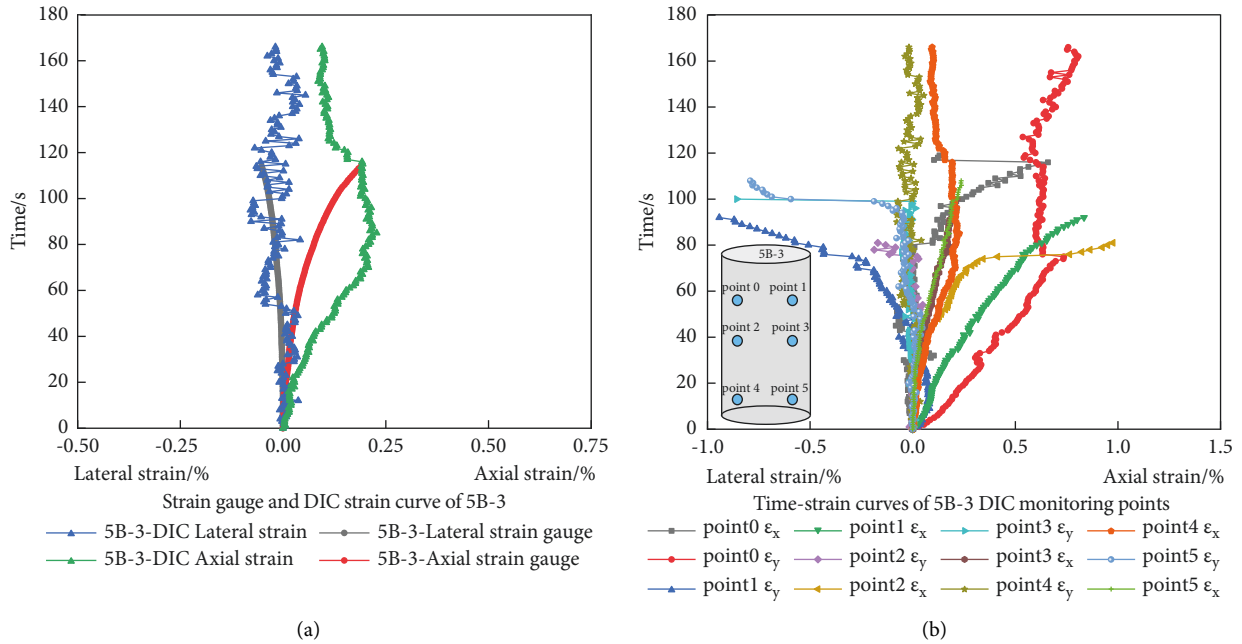

Figure 13: Time-strain curve of 5B-3. (a) Strain gauge and DIC strain curve of 5B-3. (b) Time-strain curves of 5B-3 DIC monitoring points.

Equation (7) can be obtained from the damage mechanics theory, in which σ is Stress (MPa), E is elastic modulus (MPa), and ε is strain.

$$\sigma = (1 - D)E\varepsilon. \tag{7}$$

The damage constitutive model of composite rock based on the AE ringing count was obtained by substituting Equation (6) into Equation (7). By fitting the data of S-3-AB, the trend of the stress–strain curve as shown in Figure 15 is consistent with the experimental curve, which shows that the damage model can accurately reflect the evolution process of initial damage and stable development stage of layered composite rock under uniaxial compression.

5.2. Damage Constitutive Model Based on Surface Strain of DIC. From the previous chapter 4.3, it can be seen that the dynamic evolution of strain points measured by DIC can reasonably present the damage evolution law of surface crack sprout, extension, and penetration of layered composite rocks. At the same time, the study of Zhang [13] shows that the analysis and statistics of the displacement and strain information in the full-field and the use of larger strain as the mechanical parameters to describe damage are conducive to further studying the internal relationship between the failure characteristics of rock and the damage evolution. The average value of larger strain points in the measurement area can better reflect the rock damage and the process of crack formation. The average value of strain at all points in the observation area can reasonably characterize lithology, and the difference between the two can effectively describe the evolution characteristics of rock damage. The difference between the average value of the larger strain point measured by the DIC system and the average value of all strain points is defined as the value of strain deviation $\bar{\varepsilon}$:

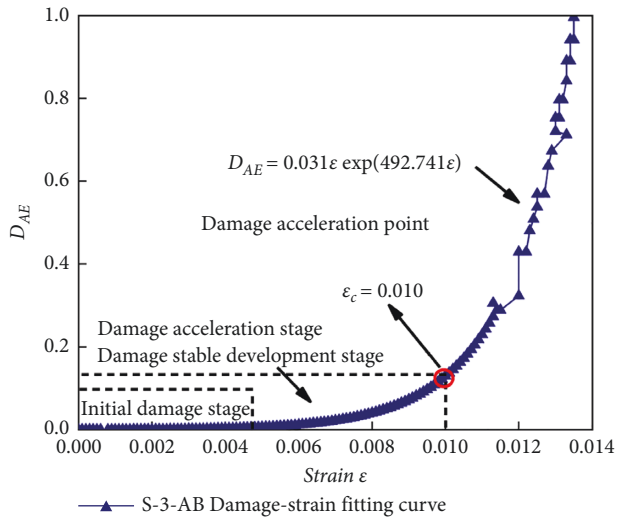

Figure 14: Damage-strain curve of S-3-AB.

$$\bar{\varepsilon} = \frac{1}{M}\sum_{i=1}^{M}(\varepsilon_1)_i - \frac{1}{N}\sum_{i=1}^{N}(\varepsilon_1)_i. \tag{8}$$

The first half of Equation (8) is the average value of M larger strain points, and the second half is the average value of N full-field strain points in the measurement area. The value of strain deviation $\bar{\varepsilon}$ is the difference between the average value of three larger strain points and the average value of six strain points in the full field. The damage factor D_f is defined as :

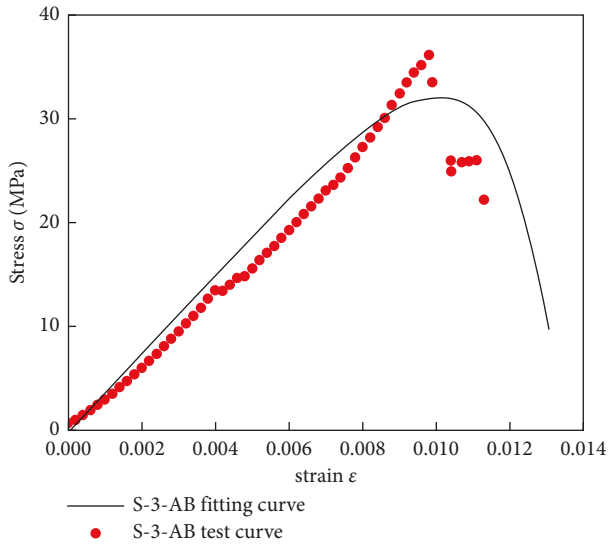

Figure 15: Test and fitted stress-strain curve of S-3-AB.

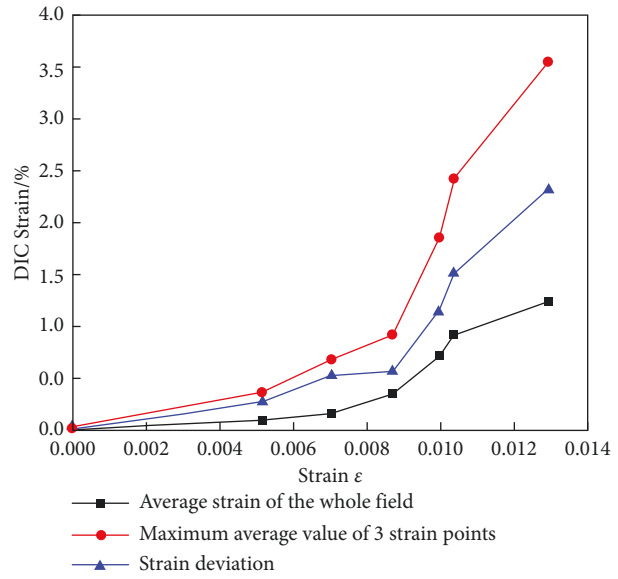

Figure 16: Variation trend of strain value measured by DIC.

$$D_f = \frac{\overline{\varepsilon}}{\overline{\varepsilon}_{\max}}. \quad (9)$$

In the Equation, $\overline{\varepsilon}_{\max}$ represents the maximum value in $\overline{\varepsilon}$.

Figure 16 shows the variation trend of the average value of the full field strain and the average value of the larger strain point measured by DIC. The percolation model was introduced and improved as :

$$D_f(\varepsilon) = |\varepsilon - \varepsilon c|^{-\alpha}. \quad (10)$$

where ε_c is the percolation threshold and α is the critical index.

By fitting the data of specimen 5A-2, obtaining that ε_c is 1.013 and α is 727.31. The damage evolution equation of damage factor D_f and strain is shown in :

$$D_f(\varepsilon) = |\varepsilon - 1.013|^{-727.31}. \quad (11)$$

The damage evolution curve of damage factor D_f and strain is shown in Figure 17. When the strain value was between 0 and 0.005, the rock was in the elastic compaction zone, the micropore was compressed and closed, and its surface had no obvious deformation. The damage factor D_f was small, which was the initial damage stage. When the strain value was between 0.005 and 0.0101, the rock turned into plastic deformation, and D_f gradually increased with the development of strain and entered the stage of stable damage development. Subsequently, D_f showed a rapid growth in a nonlinear trend after the critical strain value of 0.010. At this time, the rock structure lost its bearing capacity and produced large deformations, and entered the damage accelerated stage.

The damage constitutive model of layered composite rock based on DIC strain characteristics can be obtained by substituting Equation (11) into Equation (7). Fitting the data of 5A-2, the comparison between the fitted stress-strain curve and the test curve is shown in Figure 18. The variation trend of the stress-strain curve obtained by the damage

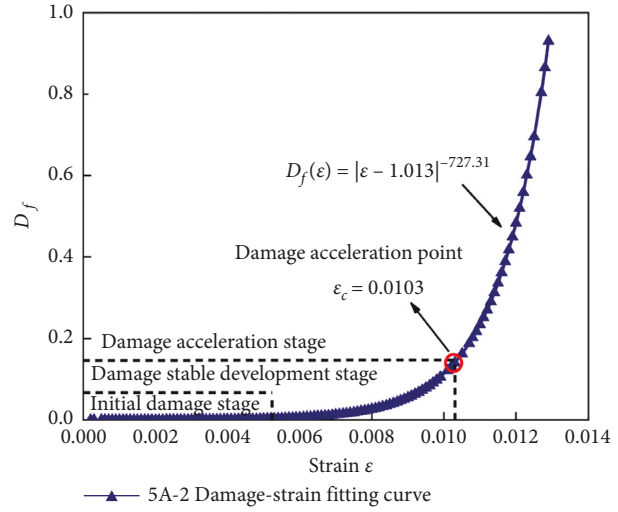

Figure 17: Damage-strain curve of 5A-2.

model fitting is consistent with the test curve, which can accurately reflect the mechanical characteristics of rock yield and post-peak large deformation stage.

5.3. Damage Constitutive Model of Layered Composite Rock Based on Dual Damage Factors Characterization of AE and DIC. The damage constitutive model based on the AE ringing characteristics and DIC surface strain has been established above. D_{AE} is a damage factor based on the AE ringing count inside the rock, which can precisely describe the initial damage and the stable development stage of the damage inside the rock. D_f is a damage factor based on the strain on the surface of the rock, and it is more appropriate to describe the peak and post-peak stages of a large strain of the rock. At the same time, a segmented curve damage model of granite had been established by Zhang et al. [34] which was based on the damage characteristics of AE and infrared

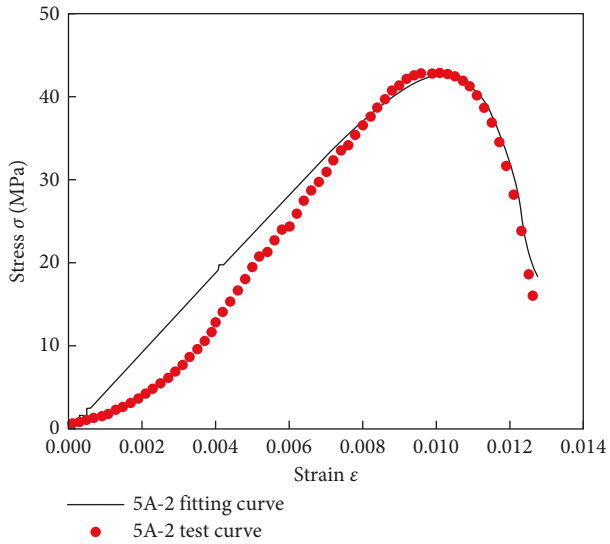

Figure 18: Test and fitted stress-strain curve of 5A-2.

characteristics and considered the complementarity of the two. Therefore, based on the advantages of AE and DIC systems in each stage, the segmented curve of the damage evolution equation was constructed in this paper to characterize the damage evolution law of rock more accurately. The damage evolution equation of layered composite rock based on a two-factor representation was as follows:

$$D = \begin{cases} \dfrac{k_1 \varepsilon \exp(k_2 \varepsilon)}{N}, & 0 \le \varepsilon \le \varepsilon_c, \\ |\varepsilon - \varepsilon c|^{-\alpha}, & \varepsilon > \varepsilon_c. \end{cases} \tag{12}$$

The damage-strain evolution equation is obtained by fitting the data of specimen 5AB-2, as :

$$D = \begin{cases} 22.477\varepsilon \exp(67.714\varepsilon), & 0 \le \varepsilon \le 0.0095, \\ |\varepsilon - 0.0095|^{-506.076}, & \varepsilon > 0.0095. \end{cases} \tag{13}$$

The damage-strain evolution curve is shown in Figure 19. When the strain was from 0 to 0.007, it was in the initial damage stage, and the primary fracture pores were closed under pressure, and the internal new fractures have not sprouted temporarily. The internal damage monitored by AE and the external strain evolution measured by DIC was not obvious, and the damage factor was small. When the strain was 0.007–0.0095, the micro-cracks inside the rock began to develop and expand, the damage gradually intensified, and the curve was steeper than the previous section. The new cracks gradually evolved on the outer surface of the rock, and the internal and external damage has accumulated. At this time, the rock was in the damage stable development stage.

When the strain was 0.0095, it corresponded to the damage mutation point, and the damage factor mutated. The rock was in the stage of damage accelerated, and large-scale cracks occurred on the outer surface of the sample, resulting in a sharp increase in the strain measured by DIC. After the damage mutation point, the damage factor rapidly

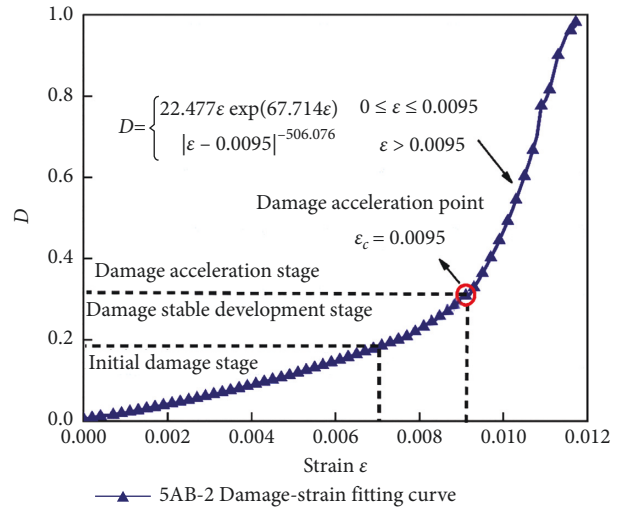

Figure 19: Damage-strain curve of 5AB-2.

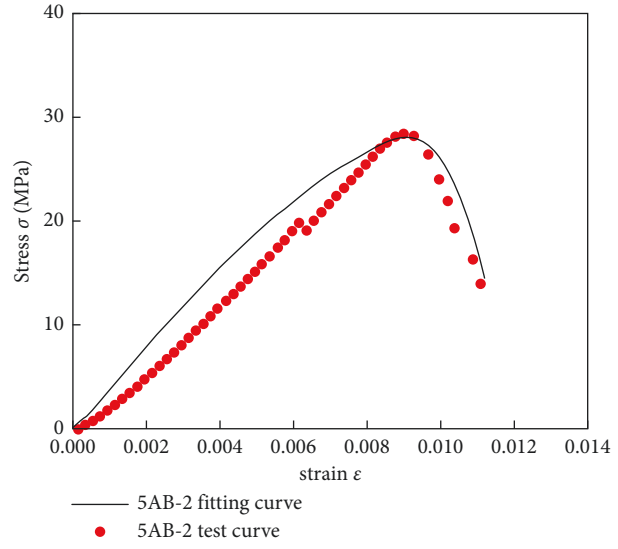

Figure 20: Test and fitted stress-strain curve of 5AB-2.

developed and approached 1 in a short-term strain, and the overall structure of the rock began to fail.

Equation (13) was substituted into Equation (7) to fit the data of specimen 5AB-2, as shown in Figure 20. The segmented fitted stress-strain curve was more consistent with the test curve. For layered composite rock, AE damage factor can better reflect the progressive failure characteristics of rock in the early initial damage stage and damage stable development stage. With a gradually increased damage, the damage variable D_f represented by DIC was more sensitive to the large strain in the later stage of rock failure.

Based on the segmental damage evolution curve characterized by daul damage factors of AE and DIC, a damage constitutive model of layered composite rock was constructed, which can reasonably embody the development of the internal structure of the rock and the damage evolution process of the germination, extension, and penetration of surface cracks. It is characterized by high damage calculation

Table 5: The feature comparison between different damage models.

Different types of damage models	Damage evolution equation	Feature analysis
Damage model defined based on the micro-defect area [32]	$D = A_d/A$	The physical meaning is clear and the form is simple, but the micro-defects are difficult to measure in the test
Damage model defined based on elastic modulus [35]	$D = 1 - (\tilde{E}/E)$	The macroscopic elastic modulus is easy to measure and widely used in practice
Damage model defined based on ultrasonic velocity [36]	$D = 1 - (V\prime/V)^2$	Operability is strong, due to rock heterogeneity resulting in low accuracy
Damage model defined based on energy change [37]	$D = (U^d/U^c)$	It is difficult to measure the energy dissipation directly, but the damage variable can be calculated accurately
Damage model defined based on strain [35]	$D = (\varepsilon/\varepsilon_s)^n$	Damage evolves as a function of strain, which can be extended from one dimension to three dimensions
Damage model defined based on DIC and AE	$D = \begin{cases} k_1\varepsilon \exp(k_2\varepsilon)/N \\ \lvert\varepsilon - \varepsilon c\rvert^{-\alpha} \end{cases}$	High calculation accuracy and complementary effects, the two can be compared and verified, and the damage can be described accurately

accuracy and complementary effects in different stress stages. Both can also be compared and verified so that the model can accurately describe the damage. The features comparison between the segmental damage model established in this paper and the damage model established by predecessors are shown in Table 5.

6. Conclusions

(1) The uniaxial strength and elastic modulus of the three types of rocks have the same variation trend. The strength and elastic modulus of type A of rock are higher than those of type B of rock by 21% and 24%, respectively, while the strength and elastic modulus of type AB of layered composite rock are slightly lower than those of type B of rock by 3% and 4%. Among the three types of rocks, the strain in the compressed density section of type AB of rock is 0.6%, while type A of rock is brittle and the strain in the compressed density section is 0.3% and type B of rock is 0.5%.

(2) Type A of rock is mainly damaged in tension, and type B of rock is mostly damaged in shear with a single inclined plane, and type AB of composite rock is mainly damaged in tension-shear slip along the bedding or weaker parts, and the strain increase also starts near the bedding after the secondary damage through the specimen, and the DIC is consistent with the strain gauges in measured whole variation pattern.

(3) According to the evolution curve of AE ringing count and stress, the AE activity of three types of rocks is weak at the beginning of loading, and the signal values reach the maximum at the peak stress. The AE ringing count value of the type A of rock is the largest, and the type B of rock is higher than the type AB of layered composite rock by 33.56%. The AE ringing signal can accurately reflect the internal damage condition with the stress development of the layered composite rocks.

(4) Based on the internal damage characteristics of AE and the damage evolution characteristics of DIC surface, a damage constitutive model of layered composite rock characterized by dual damage factors is established, which reasonably reveals the damage evolution mechanism of internal structure development and external crack germination, extension and penetration of layered composite rocks. The model is of great significance to accurately reflect the failure characteristics and damage evolution mechanism of layered composite rock and can provide a reference for the main mechanical data and failure modes of rocks in oil and gas drilling engineering

Data Availability

The data used to support the findings of this study are available from the corresponding author upon request.

Conflicts of Interest

The authors declare no potential conflicts of interest with respect to the research, authorship, and/or publication of this article.

Acknowledgments

This work was supported by the Hubei Provincial Natural Science Foundation of China (Grant no. 2020CFB367).

References

[1] Y.-J. Shen, T.-L. Rong, and G.-S. Yang, "Experimental study on ratio of quasi-sandstone similar material," *Advances in Science and Technology of Water Resources and Hydropower*, vol. 36, no. 4, pp. 75–79, 2016, (in Chinese).

[2] C. Wen, S. Jia, X. Fu, and L. Z. Meng, "Experimental research and sensitivity analysis of mudstone similar materials based on orthogonal design," *Advances in Materials Science and Engineering*, vol. 202014 pages, Article ID 2031276, 2020.

[3] P.-F. Yin and S.-Q. Yang, "Experimental study on strength and failure behavior of transversely isotropic rock-like material under uniaxial compression," *Geomechanics and Geophysics for Geo-Energy and Geo-Resources*, vol. 6, no. 3, p. 44, 2020.

[4] Q. Zheng, Y. Xu, H. Hu, and J. Y. X. Qian, "Quantitative damage, fracture mechanism and velocity structure tomography of sandstone under uniaxial load based on acoustic

emission monitoring technology," *Construction and Building Materials*, vol. 272, Article ID 121911, 2021.

[5] P. Zhang, H. Liu, K. Guan, and T. Q. Xu, "A shear model for rock microfracture size estimation based on AE measurement," *Rock Mechanics and Rock Engineering*, vol. 54, no. 5, pp. 2533–2546, 2021.

[6] X. l Li, S. j Chen, S. m Liu, and Li, "AE waveform characteristics of rock mass under uniaxial loading based on Hilbert-Huang transform," *Journal of Central South University*, vol. 28, no. 6, pp. 1843–1856, 2021.

[7] G. Zhang, Y. Xing, and L. Wang, "Comprehensive sandstone fracturing characterization: integration of fiber Bragg grating, digital imaging correlation and acoustic emission measurements," *Engineering Geology*, vol. 246, pp. 45–56, 2018.

[8] Y. Xu, Q. Zheng, X. Gao, and R. X. Q. Yang, "Quantitative damage and fracture mode of sandstone under uniaxial load based on acoustic emission," *Advances in Civil Engineering*, vol. 20209 pages, Article ID 6685795, 2020.

[9] J. Chai, Y. Liu, Y. OuYang, and D. W. Zhang, "Application of digital image correlation technique for the damage characteristic of rock-like specimens under uniaxial compression," *Advances in Civil Engineering*, vol. 202011 pages, Article ID 8857495, 2020.

[10] Y. Xue, T. Xu, W. Zhu, and M. J. Z. X. Heap, "Full-field quantification of time-dependent and -independent deformation and fracturing of double-notch flawed rock using digital image correlation," *Geomechanics and Geophysics for Geo-Energy and Geo-Resources*, vol. 7, no. 4, p. 100, 2021.

[11] J. Pan, X. Wu, Q. Guo, and X. M. Xi, "Uniaxial experimental study of the deformation behavior and energy evolution of conjugate jointed rock based on AE and DIC methods," *Advances in Civil Engineering*, vol. 202016 pages, Article ID 8850250, 2020.

[12] H. Munoz and A. Taheri, "Specimen aspect ratio and progressive field strain development of sandstone under uniaxial compression by three-dimensional digital image correlation," *Journal of Rock Mechanics and Geotechnical Engineering*, vol. 9, no. 4, pp. 599–610, 2017.

[13] H. Zhang, *Experimental Study on Damage Evolution of Quasi-Brittle Materials*, Tianjin University, Tianjin, China, (in Chinese), 2014.

[14] J.-W. Ju, G.-Z. Voyiadjis, and J.-L. Chaboche, *Damage Mechanics in Engineering Materials*, Elsevier, Amsterdam, Netherlands, 1998.

[15] A. Glema, T. Łodygowski, W. Sumelka, and P. Perzyna, "The numerical analysis of the intrinsic anisotropic microdamage evolution in elasto-viscoplastic solids," *International Journal of Damage Mechanics*, vol. 18, no. 3, pp. 205–231, 2009.

[16] R. K. Abu Al-Rub, D.-W. Lee, K.-A. Khan, and A. N. Palazotto, "Effective anisotropic elastic and plastic yield properties of periodic foams derived from triply periodic Schoen's I-WP minimal surface," *Journal of Engineering Mechanics*, vol. 146, no. 5, Article ID 04020030, 2020.

[17] R. K. A. A. Rub, "Thermodynamic framework for coupling of elasto-viscoplasticity and nonlocal anisotropic damage for microelectronics solder alloys," *International Journal of Materials and Structural Integrity*, vol. 2, no. 1/2, p. 106, 2008.

[18] W. Sumelka, M. Nowak, A. A. Nassr, H. M. T. P Al-Rifaie, and R. P. W. Studziński, "Dynamic failure of the aluminium plate under air-blast loading in the framework of the fractional viscoplasticity model - theory and validation," *International Journal of Impact Engineering*, vol. 158, Article ID 104024, 2021.

[19] O. Saeidi, V. Rasouli, R. G. Vaneghi, and R. S. R. Gholami, "A modified failure criterion for transversely isotropic rocks," *Geoscience Frontiers*, vol. 5, no. 2, pp. 215–225, 2014.

[20] S. G. Lekhnitskii and P. J. J. E. H. Fern, "Theory of elasticity of an anisotropic elastic body," *Physics Today*, vol. 17, no. 1, p. 84, 1964.

[21] L. Liu, W.-X. Zhu, and J.-F. Lu, "Research on the relationship between damage evolution and strain of stratified rock," *Chinese Journal of Rock Mechanics and Engineering*, vol. 25, no. 2, pp. 350–354, 2006, (in Chinese).

[22] J. C. Jaeger and N. G. W. Cook, *Fundamentals of Rock Mechanics*, John Wiley & Sons, Hoboken, NJ, USA, 2009.

[23] M. Bai, D. Elsworth, Z. Li, and N. Tomlin, "Evaluation of stresses and displacements induced in discretely layered media," *International Journal of Rock Mechanics and Mining Sciences & Geomechanics Abstracts*, vol. 27, no. 1, pp. 23–31, 1990.

[24] Y. M. Tien, M. C. Kuo, and C. H. Juang, "An experimental investigation of the failure mechanism of simulated transversely isotropic rocks," *International Journal of Rock Mechanics and Mining Sciences*, vol. 43, no. 8, pp. 1163–1181, 2006.

[25] D.-L. Zhao, S.-Y. Zuo, and S. Wang, "Anisotropic damage model of layered rock mass and its verification," *Science Technology and Engineering*, vol. 19, no. 11, pp. 254–261, 2019, (in Chinese).

[26] X. Li, S. Chen, S. Wang, and M. H. Zhao, "Study on in situ stress distribution law of the deep mine: taking linyi mining area as an example," *Advances in Materials Science and Engineering*, vol. 202111 pages, Article ID 5594181, 2021.

[27] Y. Gao, Y. W. Wang, and Y.-D. Wang, "Rock mechanics characteristics of lucaogou tight oil reservoir in Jimusaer sag, junggar basin," *Xinjing Petroleum Geology*, vol. 37, no. 2, pp. 158–162, 2016, (in Chinese).

[28] T. Xiao, M. Huang, and M. Gao, "Triaxial permeability experimental study on deformation and failure processes of single-fractured rock specimens," *Shock and Vibration*, vol. 202012 pages, Article ID 7329825, 2020.

[29] Cao, Lin, and Cao, "Strength and failure characteristics of brittle jointed rock-like specimens under uniaxial compression: digital speckle technology and a particle mechanics approach," *International Journal of Mining Science and Technology*, vol. 28, no. 4, pp. 669–677, 2018.

[30] Gb/T, *Standard for Test Methods Of Engineering Rock Masses*, 1999.

[31] Eitzen and Wadley, "Acoustic emission: establishing the fundamentals," *Journal of Research of the National Bureau of Standards*, vol. 89, no. 1, p. 75, 1984.

[32] L.-M. Kachanov, "Time rupture process under creep conditions," *Izvestia Akademii Nauk SSSR, Otdelenie Tekhnicheskich Nauk*, vol. 97, no. 1, pp. 11–18, 1999.

[33] Y.-J. Qin, J. Meng, and Z. Cui, "Acoustic emission damage characteristics and damage model of desert sand concrete," *Journal of China Three Gorges University*, vol. 43, no. 4, pp. 66–71, 2021, (in Chinese).

[34] Y.-B. Zhang, W.-R. Wu, and X.-L. Yao, "Acoustic emission, infrared characteristics and damage evolution of granite

under uniaxial compression," *Rock and Soil Mechanics*, vol. 41, no. s1, pp. 139–146, 2020, (in Chinese).
[35] J. Lemaitre, "How to use damage mechanics," *Nuclear Engineering and Design*, vol. 80, no. 2, pp. 233–245, 1984.
[36] T.-Q. Yu and J.-. C Qian, *Damage Theory and Applications*, National Defense Industry Press, Arlington, VA, USA, (in Chinese), 1993.
[37] R.-D. Peng, H.-P. Xie, and Y. Ju, "Research development of the rock's damage theory," *Chinese Journal of Rock Mechanics and Engineering*, vol. 26, no. 12, pp. 2526–2531, 2007, (in Chinese).